N64-16712

tech ops

TECHNICAL OPERATIONS RESEARCH

FINAL REPORT ON HYPERVELOCITY IMPACT STUDIES

(Contract NAS1-2057)

By
V. E. Scherrer and R. W. O'Neil

Report No. TO-B 63-51
21 June 1963

Submitted to

National Aeronautics and Space Administration
Langley Research Center
Hampton, Virginia

REPRODUCED BY
NATIONAL TECHNICAL
INFORMATION SERVICE
U.S. DEPARTMENT OF COMMERCE
SPRINGFIELD, VA. 22161

Burlington, Massachusetts

FOREWORD

This report was prepared by Technical Operations Research, Burlington, Massachusetts, on NASA Contract NAS1-2057.

The hypervelocity facility used for this work was developed by Tech/Ops under Contract AF33(616)-8423 as part of the hypervelocity program of the Physics Laboratory, Directorate of Materials and Processes, Aeronautical Systems Division, Wright-Patterson Air Force Base, Ohio, with Mr. A. K. Hopkins as project engineer.

The authors wish to acknowledge the support of this work by Mr. L. Salzberg, Mr. R. J. Vossler, and Mr. A. Hopkins, of the Physics Laboratory at ASD, and by Dr. F. C. Henriques, President of Technical Operations Research.

We also acknowledge the aid of Mr. F. Hauser, P. Pearsall, and R. Pelletier in carrying out these experiments.

ABSTRACT

The Tech/Ops-ASD Exploding Foil Hypervelocity Facility was used to investigate methods of accelerating spherical and cylindrical particles to velocities in excess of 60, 000 ft/sec. Targets of 2024-T3 aluminum were bombarded with two sizes of Mylar, aluminum, and copper particles. Since we discovered that some particle mass was lost during acceleration, a careful independent study was made to determine the particle mass at the time of impact.

TABLE OF CONTENTS

Chapter		Page
1	INTRODUCTION	1
2	THE HYPERVELOCITY FACILITY	2
	INTRODUCTION	2
	THE EXPLODING-FOIL GUN	4
	VACUUM SYSTEM	6
	THE ENERGY STORAGE SYSTEM	7
	DIAGNOSTIC EQUIPMENT	9
	STREAK CAMERA	10
	DYNAFAX FRAMING CAMERA	12
	CRATER MEASURING DEVICE	12
3	MEASUREMENT METHODS	14
	VELOCITY MEASUREMENTS	14
	PARTICLE MASS MEASUREMENTS	15
4	EXPERIMENTAL RESULTS	20
	METHODS OF PARTICLE ACCELERATION	20
	SPHERICAL PARTICLES	20
	DISC PARTICLES	21
	TARGET IMPACT	22
	SPHERICAL PARTICLES	22
	DISC-SHAPED PARTICLES	24
	MYLAR PARTICLES BOMBARDING 2024-T3 ALUMINUM TARGETS	24
	ALUMINUM AND COPPER PARTICLES	30
5	CONCLUSIONS AND RECOMMENDATIONS	32

LIST OF ILLUSTRATIONS

Figure		Page
1	Block Diagram of Hypervelocity System	2
2	The Gun Room	3
3	Schematic Diagram of Exploding-Foil Gun	4
4	Exploding-Foil Gun	5
5	Vacuum Chamber, Rear View (10^{-5} Torr Pressure)	6
6	Block Diagram of the Vacuum System	7
7	Equivalent Electrical Circuit of Pulsed Power Source	8
8	Energy-Storage System	9
9	Equipment Location in Hypervelocity Laboratory	10
10	Beckman & Whitley Model 339B Continuous-Writing Streak Camera	11
11	Beckman & Whitley Dynafax Framing Camera	12
12	Crater-Profile Tracing Equipment	13
13	Streak Camera, Beam Rotator, and Framing Camera	14
14	Target Recoil Configuration	17
15	Gun and Target Chamber for Recoil Studies	17
16	Conventional Gun Arrangement	20
17	Saboted Spherical Particle Gun Arrangement	21
18	Special Gun for Small-Diameter, Disc-Shaped Particles	22
19	Crater Volume as a Function of Particle Velocity for Mylar Particles Impacting 2024-T3 Aluminum Targets	26
20	NRL Observations of Hypervelocity Impact (Reprinted by Permission)	28

LIST OF ILLUSTRATIONS

Figure		Page
21	Comparison of Tech/Ops Data with NRL Data	29
22	Depth of Penetration of Mylar Particles Bombarding 2024-T3 Aluminum Targets	30

LIST OF TABLES

Table		Page
1	Summary of Particle Mass Measurements	19
2	Summary of Mylar Particle Impact Data on 2024-T3 Aluminum Targets	25
3	Summary of Aluminum Particle Impact Data on 2024-T3 Aluminum Targets	31
4	Summary of Copper Particle Impact Data on 2024-T3 Aluminum Targets	31

CHAPTER 1

INTRODUCTION

The purpose of Contract No. NAS1-2057 was to use the Tech/Ops-ASD Hypervelocity Facility to demonstrate that single intact projectiles could be accelerated to speeds in excess of 60,000 ft/sec by means of electrically exploding wires and foils. Both spherical and disc-shaped projectiles were investigated.

We contracted to carry out a series of at least eighteen target impacts for those experimental conditions that were successful. In particular, 2024-T3 aluminum targets were to be bombarded with glass, aluminum, and copper particles having masses ranging from 0.1 mg to 18.2 mg. If possible, the particles were to be spheres 1/64 in. and 1/16 in. in diameter. Impacts were to be made in the following velocity regions:

Between 15,000 and 20,000 ft/sec

Between 25,000 and 40,000 ft/sec

At the highest possible velocity above 50,000 ft/sec.

An extensive research program of over 300 shots was accordingly carried out to study methods of accelerating spheres and small-diameter disc-shaped particles. Since our standard gun is normally used only for disc-shaped particles 1/4 in. in diameter, a number of special guns were designed for the spherical particles and for small disc particles (less than 1/8 in. diameter). (Each of the methods of particle acceleration will be described in Chapter 4.) Particle velocities were measured with a Beckman & Whitley Model 339B Continuous-Writing Streak Camera.

We have found, in other work, that some mass is lost from the particle during acceleration to hypervelocity. Therefore, approximately 100 shots were fired in studies of momentum transfer to targets, to experimentally measure the particle mass just prior to impact.

Since our interpretation of the data depends on the experimental methods used, we shall first describe the hypervelocity facility (Chapter 2) and the methods used to measure the particle velocity and particle mass (Chapter 3) before presenting the data (Chapter 4). Recommendations for future work will be made in Chapter 5.

CHAPTER 2

THE HYPERVELOCITY FACILITY

INTRODUCTION

The Tech/Ops-ASD Hypervelocity Facility consists of an expendable, exploding-foil gun, an electrical energy-storage system, a vacuum system, and associated diagnostic equipment: a Beckman & Whitley streak camera, a backlighting source, a Beckman & Whitley Dynafax camera, and crater-profile tracing equipment. A block diagram of the overall system is shown in Figure 1.

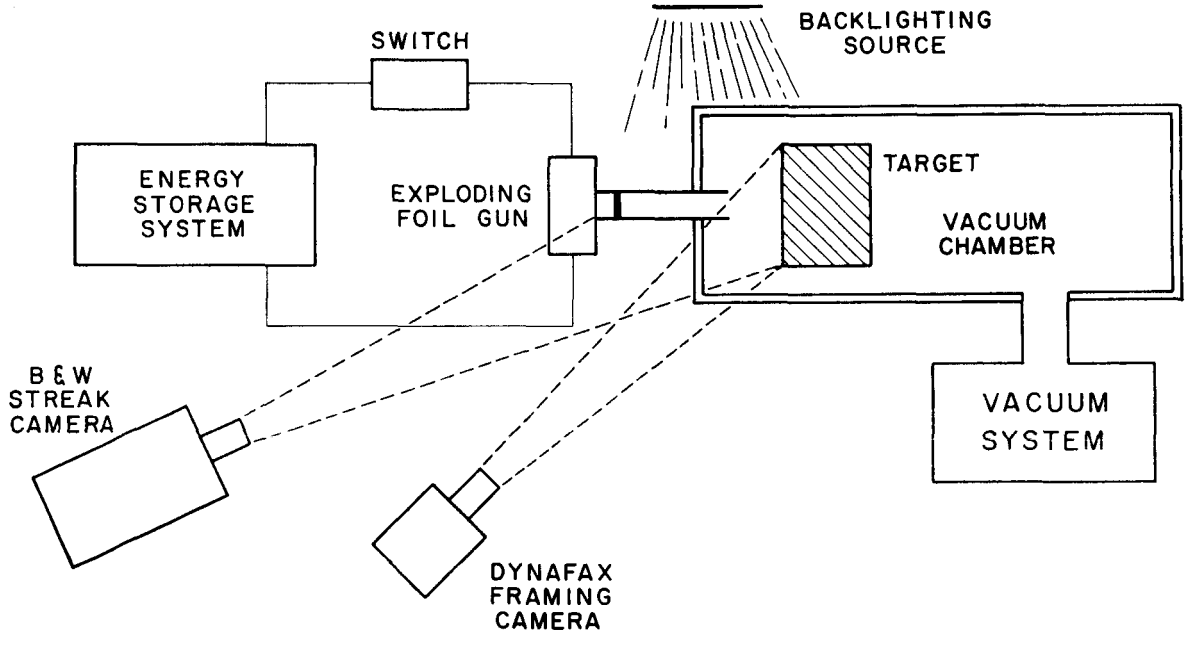

Figure 1. Block Diagram of Hypervelocity System

In operation, foil is placed in the breech area of the gun, which is exploded by an electrical discharge from the energy storage system. The hot gas generated by the explosion "punches" a particle from a Mylar diaphragm stretched across the accelerator tube and expels it from the gun. The particle then bombards the target. The diagnostic equipment records phenomena during impact, such as the light emitted and particle velocity. Other effects of target impact, such as crater volume, are measured later with the profile tracing equipment.

A separate gun room houses the vacuum chamber and exploding-foil gun, to protect equipment and personnel from debris during the gun explosion. Figure 2 is a side view of the gun room showing the plastic window through which experiments are viewed and recorded by the Beckman & Whitley Model 339B Continuous-Writing Streak Camera.

We will now describe each component of this system in more detail.

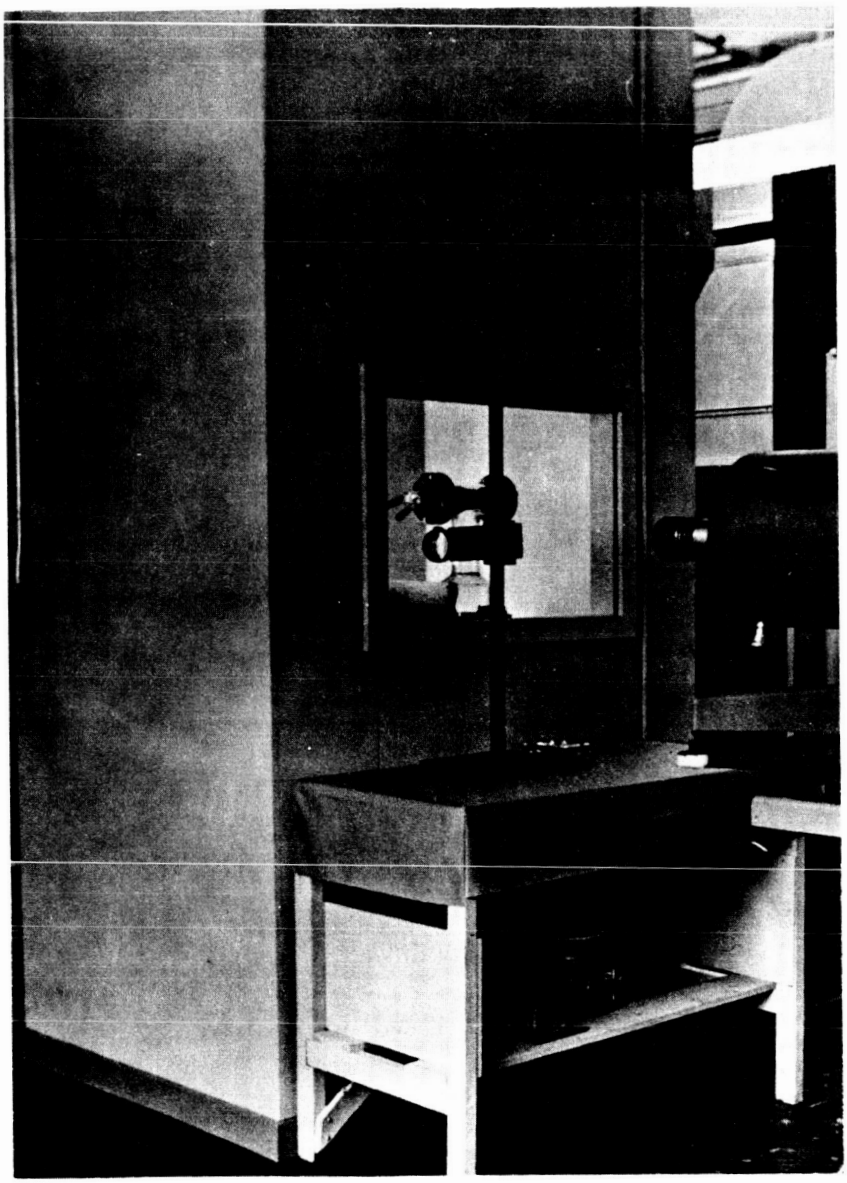

Figure 2. The Gun Room

THE EXPLODING-FOIL GUN

The "gun" used in these experiments consists essentially of an electrically exploded foil as the "explosive charge," a solid plastic as the "breech," and a plastic capillary tube as the "barrel." A schematic diagram of one arrangement of the experimental gun is shown in Figure 3.

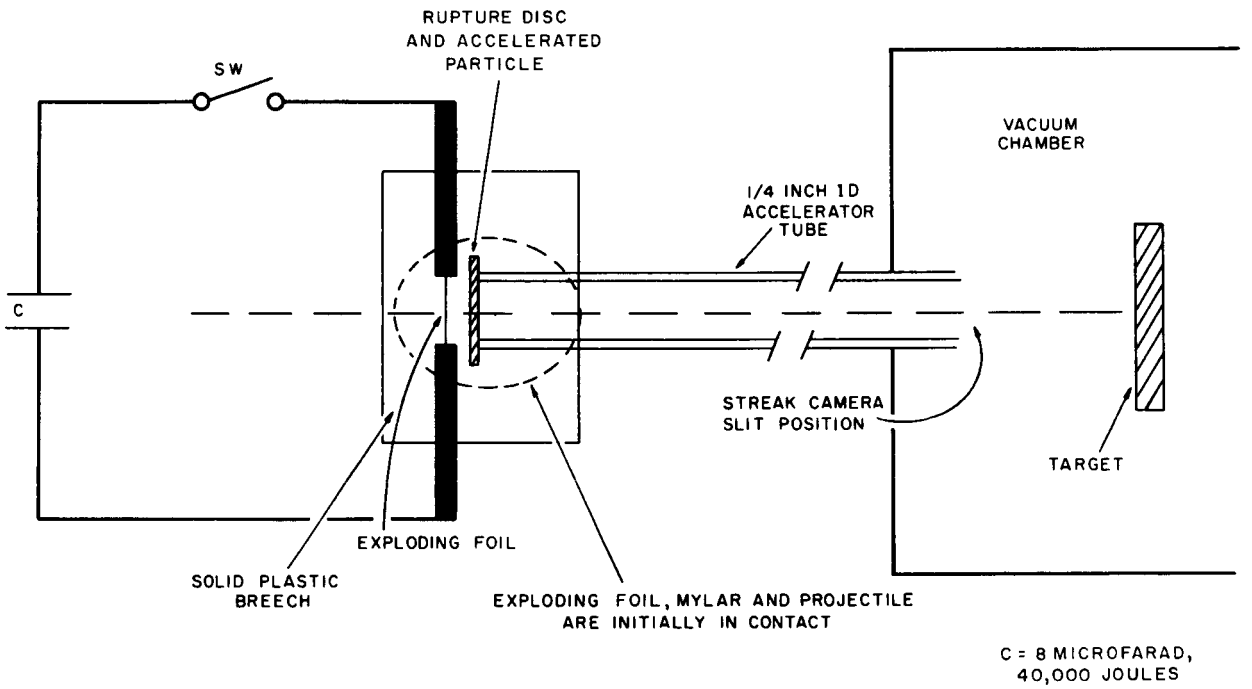

Figure 3. Schematic Diagram of Exploding-Foil Gun

The electrical explosion is separated from the accelerator tube ("gun barrel") and vacuum chamber by a Mylar diaphragm (rupture disc), which confines the explosion for a time interval approximately equal to the effective discharge time of the electrical circuit. The diaphragm then ruptures, forming a disc-shaped particle which fits the barrel very tightly and provides a good gas seal. The hot propellant gas then expands and expels the particle from the accelerator tube, which is mounted in a large glass vacuum chamber containing the target.

When plastic particle materials other than Mylar are used in the gun, the Mylar diaphragm is replaced by the plastic material. When metal particles are accelerated, electrical insulation must be provided between the metal diaphragm and the electrically exploding foil. We have found that a Mylar sheet 2 mils thick gives sufficient insulation. We believe that this film is mostly vaporized during the electrical explosion.

The diameter of the gun barrel can be varied, thereby varying the diameter of the accelerated particle. Barrel diameters (inner) of 1/8 in. to 1/2 in. have been successfully used. For a given particle diameter, the particle mass can also be varied by changing the thickness of the "rupture disc." Disc thicknesses from 0.005 in. to 0.050 in. have proved successful.

Figure 4 shows an expendable gun in an unmounted position. This particular gun used a Mylar disc 0.010 in. thick. The inner diameter of the barrel was 0.25 in. The foils extending from either side of the gun are electrical connectors.

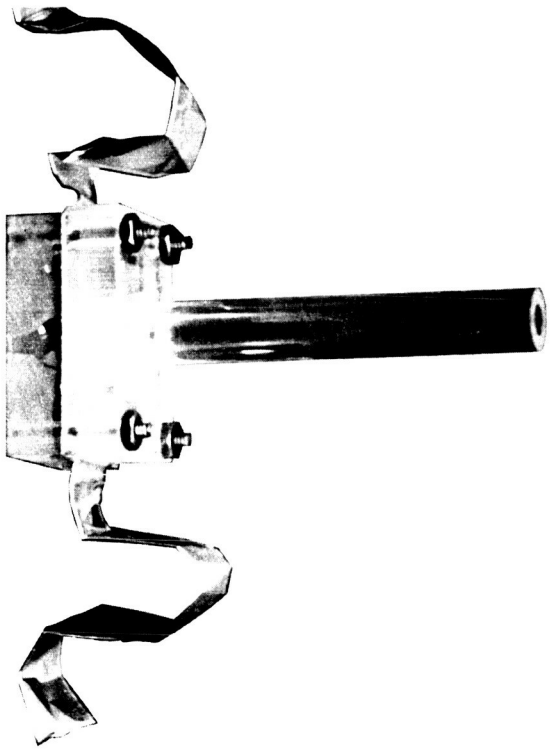

Figure 4. Exploding-Foil Gun

Figure 5 shows the vacuum chamber. It is constructed of doubly tough pyrex glass, 6 in. in diameter, and is connected to a vacuum system capable of evacuating the chamber to an ambient air pressure of 10^{-5} Torr. A copper pipe, 4 in. in diameter, extends from the vacuum chamber to the vacuum system outside the gun room. The vacuum chamber is viewed from the rear entrance door of the gun room in this picture. The gun is inserted through the metal flange on the right side of the chamber.

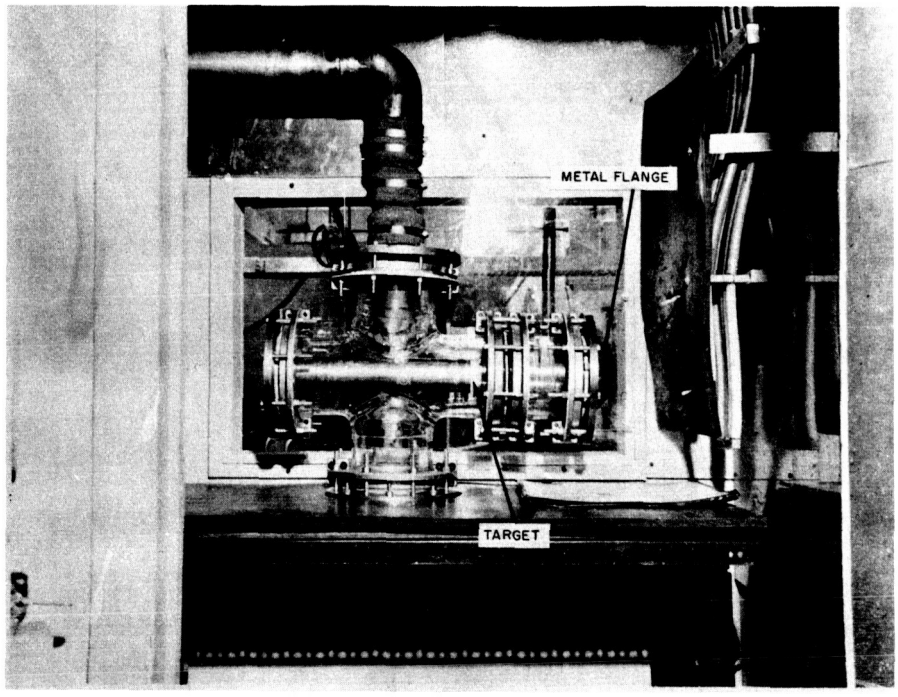

Figure 5. Vacuum Chamber, Rear View (10^{-5} Torr Pressure)

VACUUM SYSTEM

The vacuum system, a standard 4 in. commercial system, consists of a mechanical fore pump, a diffusion pump, a gate valve, and a 4 in. pipe. To this system we have added a liquid-nitrogen cold trap near the vacuum chamber. A schematic diagram of the vacuum system is shown in Figure 6.

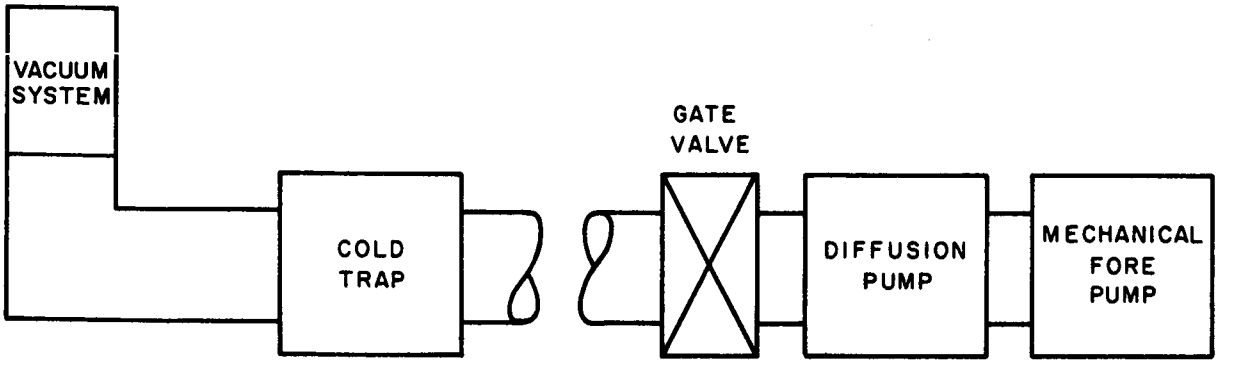

Figure 6. Block Diagram of the Vacuum System

THE ENERGY STORAGE SYSTEM

In the past, chemical explosive systems have been primarily used in ballistics research. In our system, we have substituted electrical for chemical explosions, since electrical explosions give greater control over energy input and generate higher energy densities in the propellant material. The resulting high temperatures enable us to obtain higher particle velocities than in conventional chemical guns.

The energy storage system consists of two banks of capacitors of the best available commercial type. Each bank is a parallel connection of eight 1 μF capacitors, with each capacitor capable of storing 5,000 J of electrical energy at a potential of 100 kV. The capacitors are guaranteed to last for 1000 shots at full energy when discharged through a load for which the peak-to-peak voltage across the capacitor during discharge does not exceed 180 kV. The capacitors are guaranteed for an additional 10,000 shots when charged to 50 kV. At this voltage, the capacitors store 1250 J each. Since we expect to fire this facility greatly in excess of 1000 shots over a period of several years, we have given the capacitor bank a rating of 10,000 J at 50 kV. The estimated effective discharge time for the system when coupled to a matching resistive load is 5 μsec.

Figure 7 is a schematic diagram of the equivalent electrical circuit. Energy stored on the energy storage bank, C, is discharged through the hypervelocity-gun load transducer, R_L, when the reduced-pressure switch, SW, is triggered by pumping air from it, thereby reducing the dielectric strength of the residual air. (An electronically triggered switch will be installed.) The capacitor, C, in Figure 7

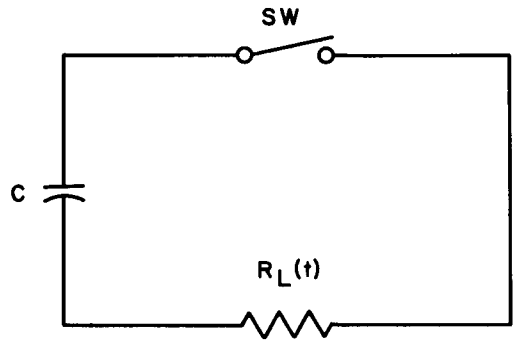

C = 8 μF 100 kV, 16 μF 100 kV, or 4 μF 200 kV

$R_L(t)$ = time-dependent exploding-foil resistance

Figure 7. Equivalent Electrical Circuit of Pulsed Power Source

represents a single capacitor bank (8 μF 100 kV), a parallel connection of two capacitor banks (16 μF 100 kV), or a series connection of two capacitor banks (4 μF 100 kV). For a single capacitor bank, the effective discharge time is approximately 5 μsec. Since a substantial part of the total circuit inductance is located in the gun and its connecting leads, the parallel connection of two banks gives a somewhat slower discharge than a single bank, and a series connection gives a slightly faster discharge.

Figure 8 shows the energy-storage system with the component parts indicated. Parallel-plate connectors with Mylar insulation between the plates (a good method of connecting capacitors of this type) are used. Figure 9 illustrates the location of the energy-storage system relative to the gun room, gun vacuum chamber, vacuum system, and streak camera.

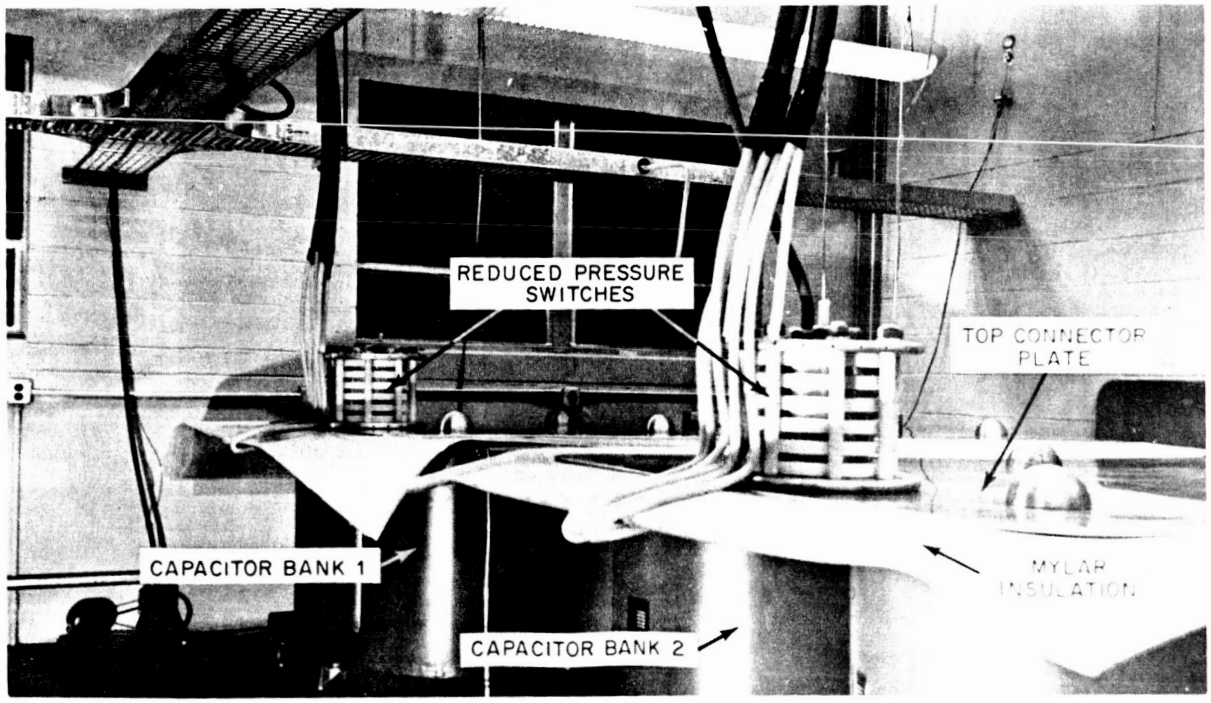

Figure 8. Energy-Storage System

DIAGNOSTIC EQUIPMENT

The diagnostic equipment consists of a Beckman & Whitley Model 399B Continuous-Writing Streak Camera, a backlighting source, a Beckman & Whitley Dynafax Framing Camera, and crater-profile tracing equipment. The streak camera and the backlighting source record the details of the initial explosion and the performance of the exploding-foil gun, and yield measurements from which particle velocities are determined. The Dynafax camera is used for dynamic studies of target impacts (i.e., recoil velocity of target in a frictionless mount), and the crater-profile tracing equipment is used to study the final results of impact.

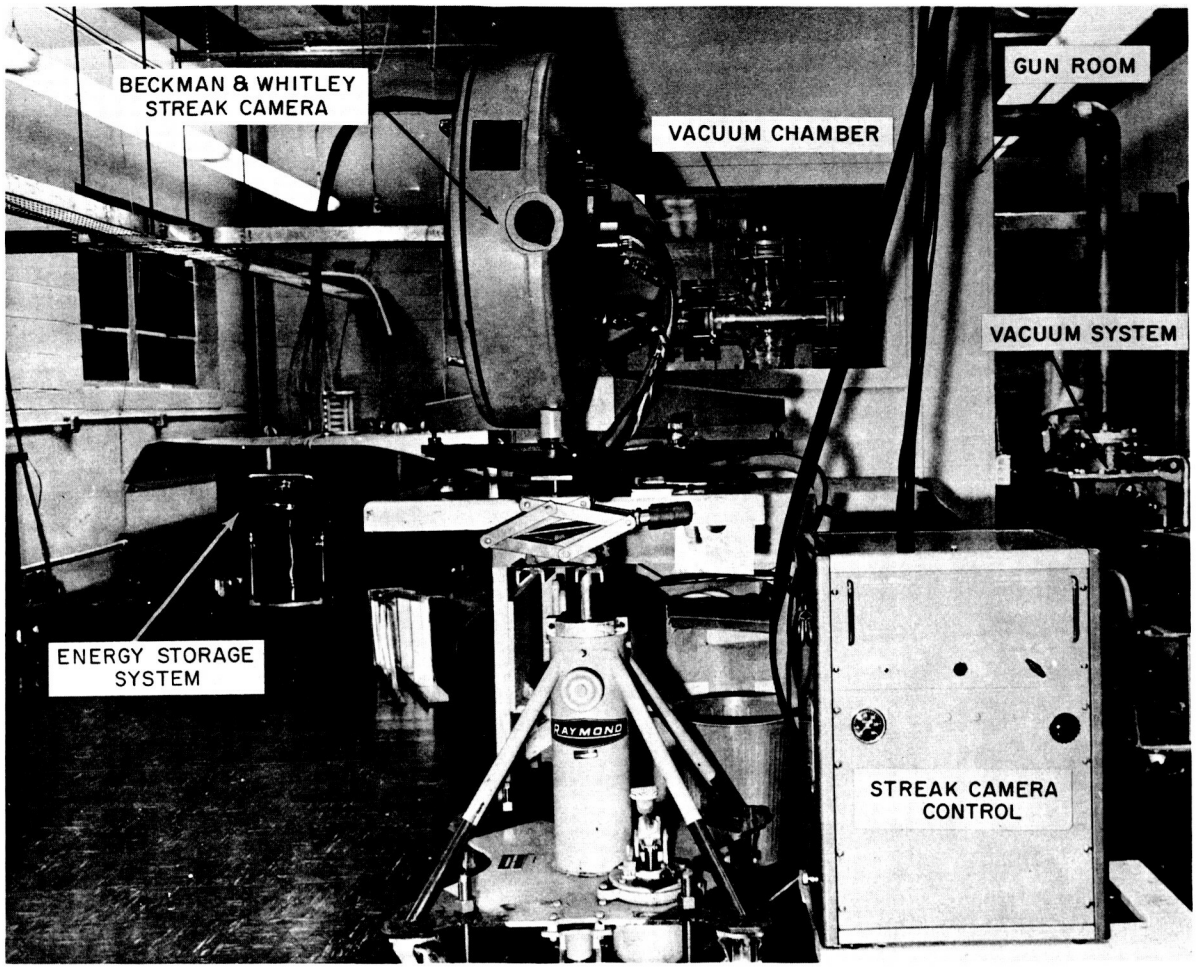

Figure 9. Equipment Location in Hypervelocity Laboratory

STREAK CAMERA

The Beckman & Whitley streak camera is a research instrument employed in the study of high-speed events. The camera transcribes (on 35 mm film) information which is a variable density record of the illumination falling upon a slit as a function of time. The film is stationary and is swept by the traveling slit image reflected by a rotating mirror. The image of the event is placed on the slit aperture by the objective lens. The internal relay optics are of first-surface mirror construction and give highest resolution to the image reflected onto the curved film track by the rotating mirror in the evacuated body of the camera.

The internal optical system of the camera reduces the image by a factor of 2. We are presently using a 12-mil slit. For this slit, the time resolution at the maximum writing rate of 9.1 mm/μsec is 1.6×10^{-8} sec.

The rotating mirror is an aluminized, three-face, optical-quality beryllium mirror driven by a turbine. Nitrogen gas drives the turbine to a maximum speed of 2600 rps, giving a maximum writing rate of 9.1 mm/μsec on the film. Air friction is greatly reduced by evacuating the entire camera housing to a vacuum of 1.5 in. of mercury. The camera is operated from a remote control unit which contains the turbine and shutter controls and an electronic counter. The counter gives a direct read-out of turbine speed in revolutions per second. Figure 10 shows the streak camera set-up to view the exploding foil gun through the plastic window in the gun room.

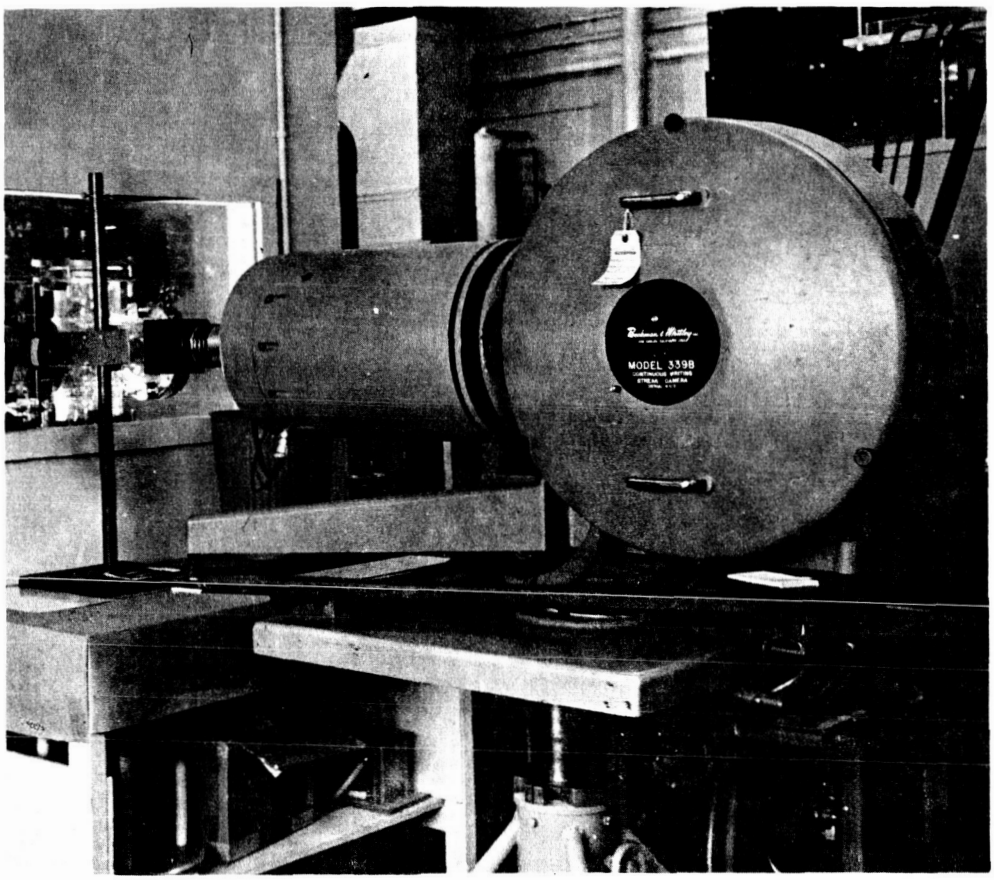

Figure 10. Beckman & Whitley Model 339B Continuous-Writing Streak Camera

DYNAFAX FRAMING CAMERA

The Beckman & Whitley Dynafax Camera in Figure 11 is used primarily for observing slow moving events associated with target impacts. It has a maximum framing rate of 25,000 frames/sec.

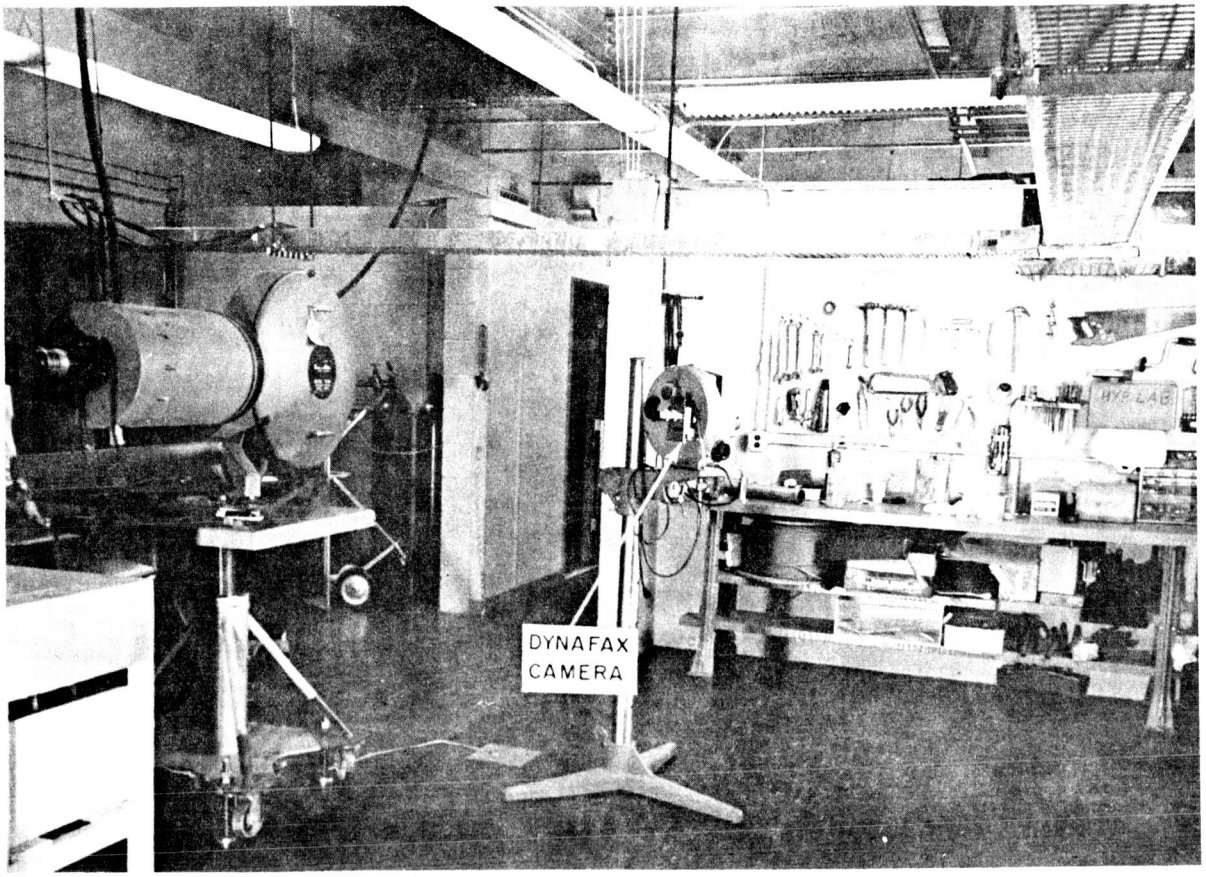

Figure 11. Beckman & Whitley Dynafax Framing Camera

CRATER MEASURING DEVICE

Figure 12 shows the device used to measure the depth and diameter of the target craters resulting from hypervelocity impact. It consists of a precision micrometer crossfeed table and long-reach dial indicator that permit depth measurement to within 0.001 in. and diameter measurements, in two directions, to within 0.0001 in. Volume measurements are made with micropipettes to within 0.001 cm^3.

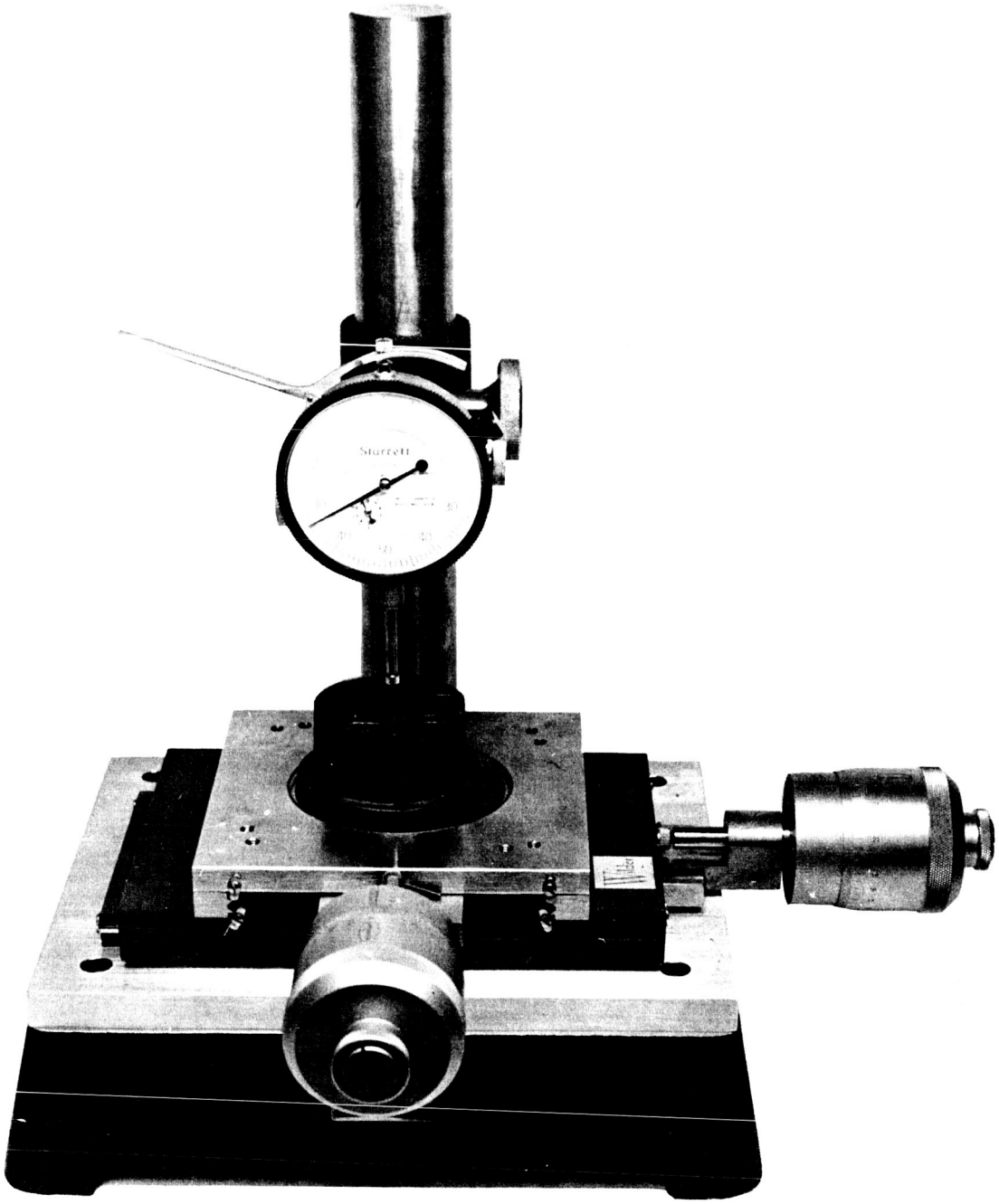

Figure 12. Crater-Profile Tracing Equipment

CHAPTER 3

MEASUREMENT METHODS

VELOCITY MEASUREMENTS

Incident particle velocity is determined with a Beckman & Whitley Continuous-Writing Streak Camera, in which horizontal displacement is recorded as a continuous function of time. Since the gun is fired vertically in this experiment, the optical beam must be rotated through an angle of 90^{o} by using a system of mirrors. The streak camera and beam rotator are shown in Figure 13. Also shown in the picture is a 25,000 frame/sec continuous-writing framing camera, which is used for target recoil studies.

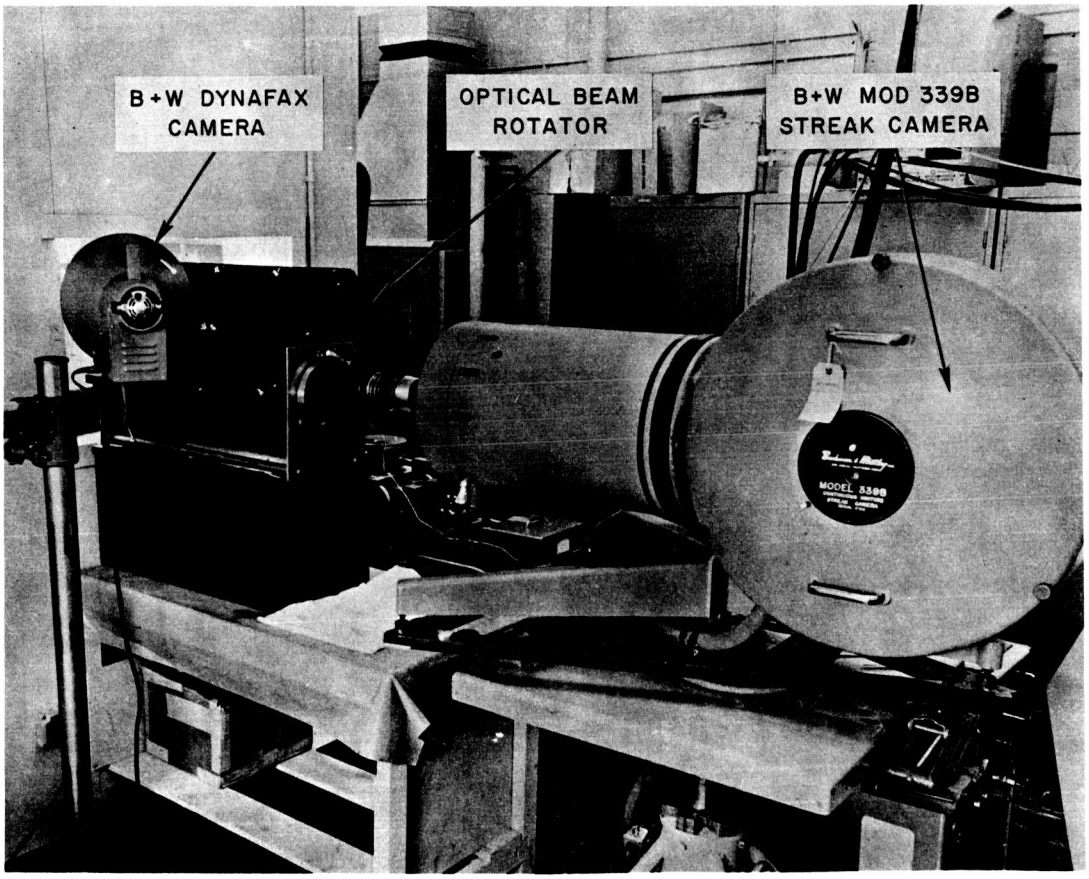

Figure 13. Streak Camera, Beam Rotator, and Framing Camera

With the streak camera, it is possible to obtain time resolutions of 9.1 mm/μsec in a well-lighted field, and since this experiment uses a very intense plasma as a particle propellant, velocities are recorded on well-exposed, highly resolved photographic films. More than 3000 streak films have been analyzed during the development of this experiment, and it is unreasonable to expect an analysis error of more than 2-1/2% for a well-exposed film.

PARTICLE MASS MEASUREMENTS

To determine the impacting mass of a particle fired in our gun, momentum-transfer measurements must be made, since it is impossible to weigh the actual particle either before or after the shot. In our standard projection technique (Chapter 2), a disc-shaped particle the same size as the "gun barrel" is punched out of a Mylar diaphragm of uniform thickness. After a shot, a perfect disc-shaped hole is found in the recovered remnant of the larger piece, and the uniformity of the impact indicates that the explosion breaks out a single, uniform, disc-shaped particle. However, during the few microseconds that the disc is accelerated, it is subject to extreme temperature gradients and "barrel friction," and it is reasonable to expect that some ablation could take place early in the acceleration phase. To determine the extent of any possible particle mass losses, a method of measuring the momentum transfer of the particle has been implemented.

It had been suggested that this momentum might be measured with a ballistic pendulum, but when the difficulties involved in data measurement, compensation for background, and late time effects peculiar to this gun were evaluated, the more direct technique of measuring target-recoil velocity was chosen. A primary consideration in this choice was the necessity to eliminate the air inrush caused by the breakdown of the vacuum in the gun chamber after each shot. The reaction time for a ballistic pendulum is longer than the time it takes the air inrush to reach the target ($\approx$10 - 20 ms), and the only way to eliminate these air effects is to enclose the entire operation in a fairly large vacuum chamber. Such a facility modification was not practical for this contract, and with a properly designed target-recoil system, air inrush is not a serious problem. A fast-rising (< 5 μsec), short-duration ($\approx$ 5 ms) target backlighting source completely eliminates this effect from the experiment.

The method chosen for the target recoil studies features a low density target designed to trap the momentum of a particle of a given mass and velocity. This target design (see Figure 14) uses a very light canister that is filled with a predetermined number of thin aluminum sheets (0.005 in. → 0.010 in.) and relatively thick Styrofoam absorbers. The weight of these targets can be varied from 1 to 20 g as the particle material and velocity range is changed.

The open end of the target is covered with a thin foil Mylar laminate (0.003 in. total thickness) that allows the particle to enter the target easily but is strong enough to eliminate target-mass losses during impact and to trap any recoil momentum (except for that lost out the small hole through which the particle enters) resulting from flash vaporization and hydrodynamic blowoff. At each interface the particle loses some mass as vapor and small fragments, and these are captured by the absorbing material.

By this technique, the normal momentum is conserved without introducing additional accelerations. Measurements are taken in the vertical direction in less than 2 ms over distances of about 2 cm. The target velocities are measured with a Beckman & Whitley Dynafax Framing Camera, which can take 224 well-resolved data frames in times as short as 9 ms (see Figure 15). For analysis, each frame is magnified 20 times, and 98% accuracy is possible in target velocity determination.

If a target velocity of 1290 cm/sec were measured for a 13.00g target, this would correspond to an incident momentum of 1.68×10^4 g cm/sec. Given a measured particle velocity of 50,000 ft/sec, the calculated mass would be 11 mg if perfect efficiency were assumed. There will be some losses in momentum transfer and slight errors in incident velocity measurement ($\pm$ 2.5%) but an accuracy of $\pm$5% can be achieved. Uncontrollable differences in the construction of the individual guns makes it difficult to predict exactly what the velocity, mass, or momentum will be for a particular shot, but large numbers of shots and careful measures taken to ensure uniformity permit a valid statistical evaluation of data.

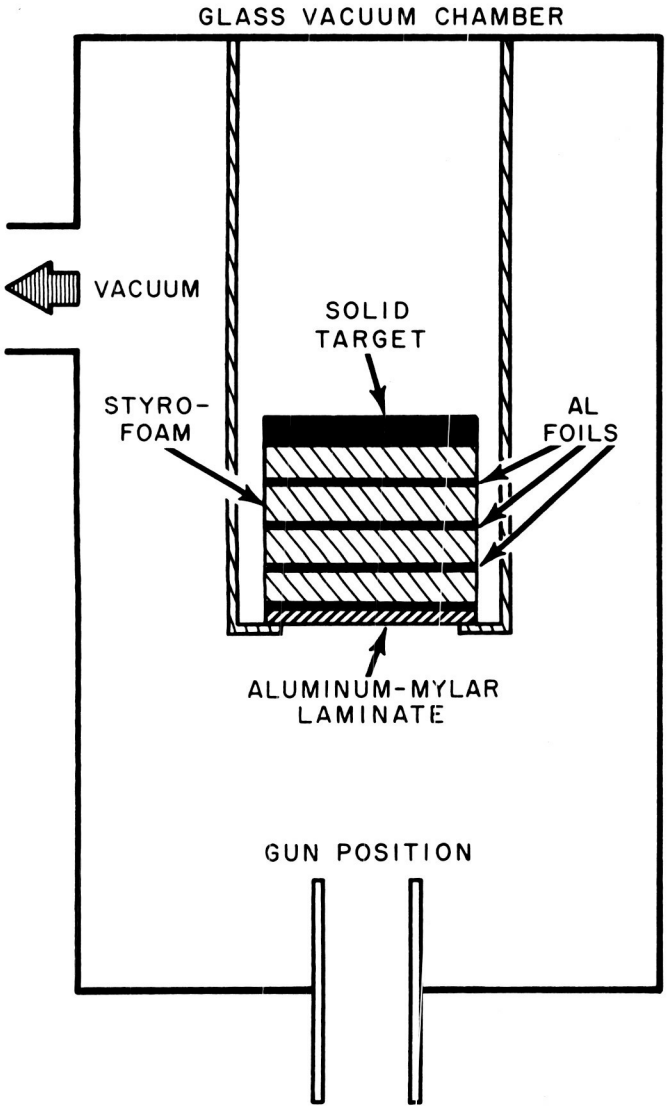

Figure 14. Target Recoil Configuration

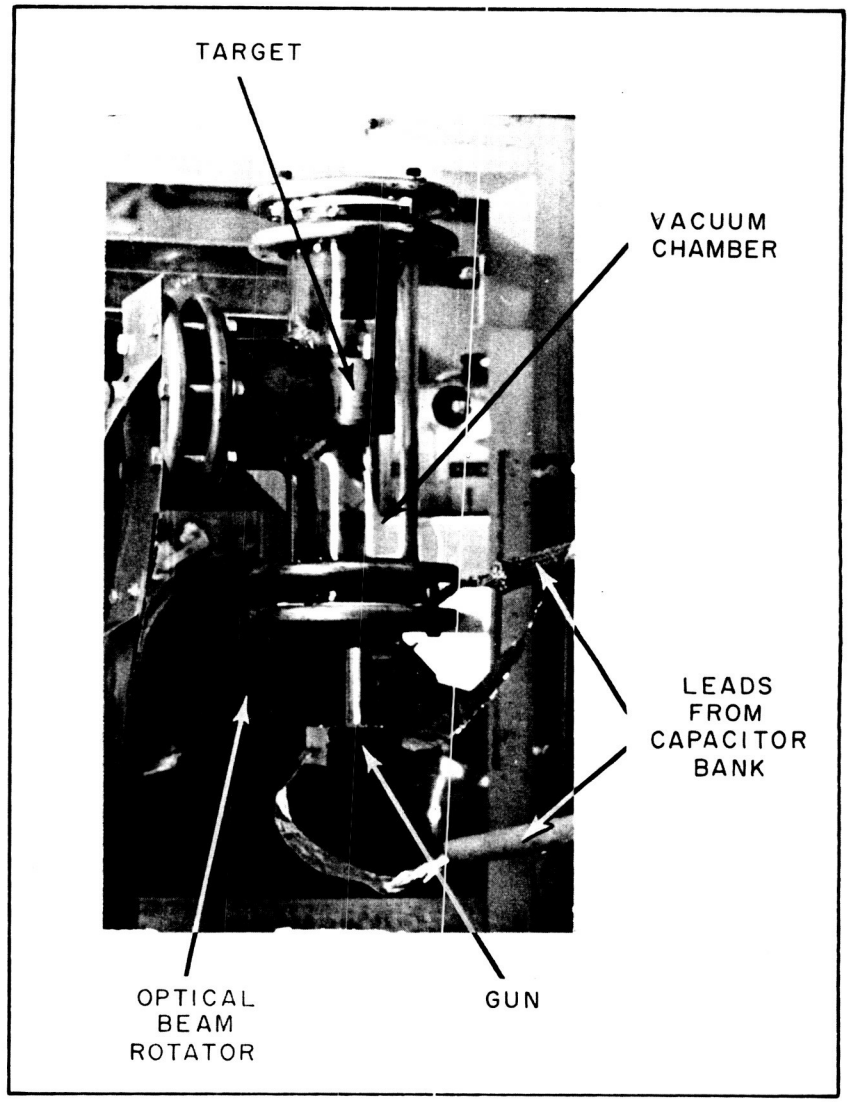

Figure 15. Gun and Target Chamber for Recoil Studies

tech/ops

At the present time, particle mass is determined from the momentum transfer equation in the form

$$m = \frac{MV}{v}$$

where

m = particle mass

M = the weighed target mass

V = the target velocity measured from framing camera picture

v = the incident particle velocity measured from streak pictures.

In this form no effort is made to compensate for target mass losses, or the initial explosive reaction occurring when the particle first enters the target. These effects are small and very difficult to evaluate exactly, but any correction for them would reduce the calculated particle mass by some small and near constant factor.

To assure that propellant plasma and other debris were not affecting the measurement, "background" shots were fired. The guns were identical in all respects with those used in shots described above, but no particle was loaded into the gun. In all cases, the momentum of the plasma was lower than that of the particle by a factor of 10, although the plasma velocities were 2 to 3 times faster than the highest particle velocities.

Additional shots were fired when the target for measuring impacting mass was located only 1 cm from the end of the gun barrel. Under these circumstances, the target is bombarded by the particle plus all the propellant gas. We obtained an impacting mass that was approximately equal to the initial particle mass in these measurements. Since the mass of the exploding foil is negligible compared to that of the particle, we can account for all the mass before the particle was vaporized. This measurement supports our particle-velocity measurement.

In our effort to duplicate the particle masses specified in the contract — 0.1 mg to 18.2 mg — we assumed that the impacting mass of the particle would be in a constant proportion to the initial mass. However, our target recoil measurements showed that this is not the case. A copper disc that originally weighed 37.9 mg lost nearly 80% of its initial mass as vapor before hitting the target. A similar aluminum disc lost 55%, and a Mylar disc 45%. Shearing properties, elasticity, vaporization energy, confinement time, and several other factors enter in a complex way to yield the differences in mass loss percentage.

For each particle material, sufficient numbers of shots were fired under identical circumstances to determine a valid statistical value for the impacting mass of the particle. Each of these shots was evaluated carefully to eliminate doubtful impact velocities, possible particle breakup, and other irregularities. The masses for the particles fired, as calculated by the method indicated above, are given below in Table 1. The number of shots, average mass, and the mean square deviation are also included.

TABLE 1

SUMMARY OF PARTICLE MASS MEASUREMENTS

Material	Disc		Initial Mass (mg)	Impacting Mass (mg)	Number of Shots Averaged*
	Diameter (in.)	Thickness (in.)			
Aluminum	0.250	0.005	13.0*	6.04 ± 0.545	9
Copper	0.250	0.005	37.9*	6.98 ± 0.890	26
	0.120	0.005	8.20*	1.64 ± 0.16	
Mylar	0.250	0.010	11.0	6.06 ± 0.126	17
	0.125	0.010	2.75	1.43 ± 0.022	13

*Includes 0.002 in. insulation.

CHAPTER 4
EXPERIMENTAL RESULTS

METHODS OF PARTICLE ACCELERATION

The acceleration of spherical particles and discs having diameters less than 1/8 in. required the development of a number of gun geometries in addition to the standard gun shown in Figure 3.

SPHERICAL PARTICLES

The conventional gun geometry for spherical particles shown in Figure 16 is very similar to our standard gun. The rupture disc is replaced by a thinner insulating disc (Mylar 2 mils thick), and a spherical particle is glued to the front surface of the disc. The spherical particle fits loosely in a reamed plastic tube. This geometry has several disadvantages relative to our standard gun. One disadvantage is barrel friction and propellant gas leakage past the particle. Another is the larger

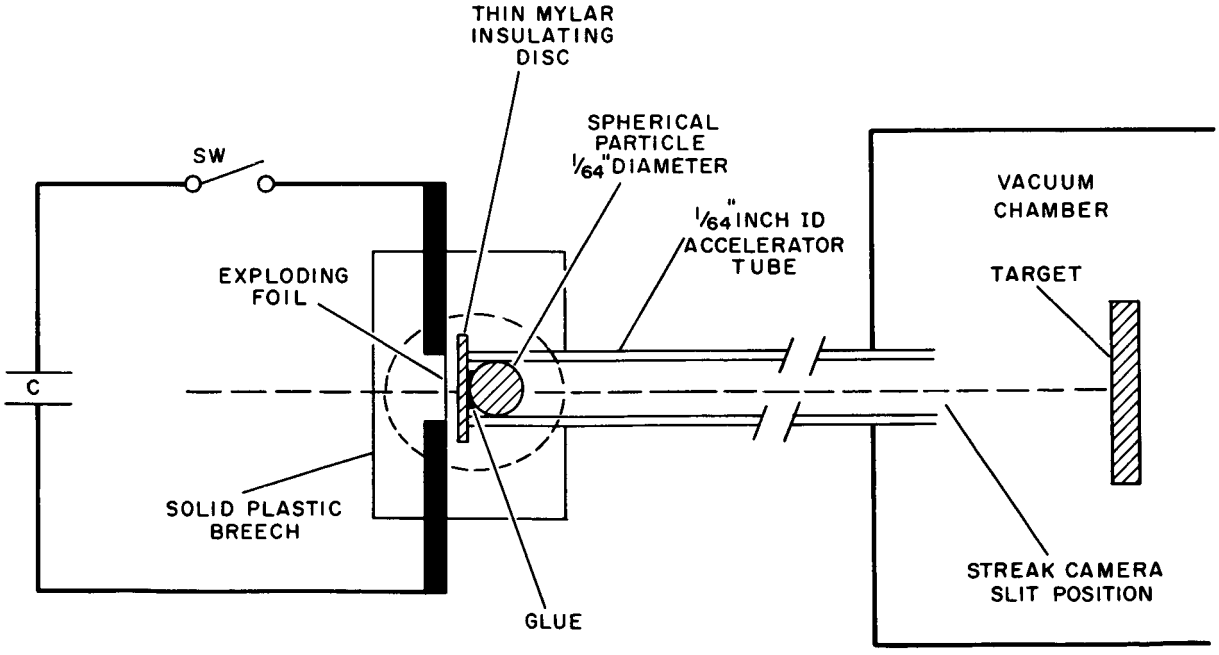

Figure 16. Conventional Gun Arrangement

mass per unit area of the particle, without increased energy per unit area of the propellant gas. The "challenge" of this arrangement is to increase the propellant gas temperature and energy density.

Figure 17 shows a second gun geometry that was used for the projection of spherical particles. Here the basic geometry is the same as our standard gun except that a small spherical particle is glued to the front surface of a sabot, 1/4 in. in diameter and 10 mils thick. (The sabot is the particle in our standard gun.) A steel aperture plate is used to stop the sabot and allow the particle to pass through.

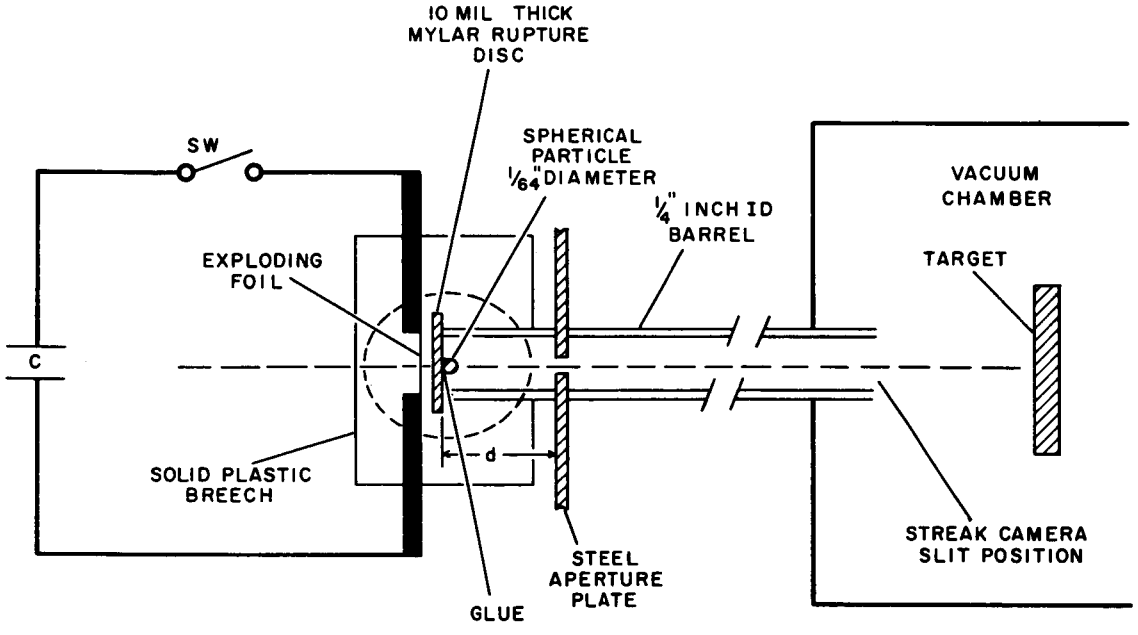

Figure 17. Saboted Spherical Particle Gun Arrangement

DISC PARTICLES

Normally, our standard gun is used only for particles that are disc-shaped and 1/4 in. in diameter. To accelerate particles having diameters less than 1/4 in., a circular groove about 5 mils deep and with a diameter equal to the inner diameter of the barrel is cut in the rupture disc. This configuration is used for particle diameters between 1/8 in. and 1/4 in.

The geometry shown in Figure 18 is used for disc-shaped particles having diameters less than 1/8 in. The arrangement is the same as the standard gun except that a sharpened steel tube is placed against the rupture disc to punch out the disc-shaped particle. If the rupture disc is metal, it is insulated from the electrical explosion with 2 mil Mylar sheet. The geometry has been used for particle diameters as small as 0.080 in.

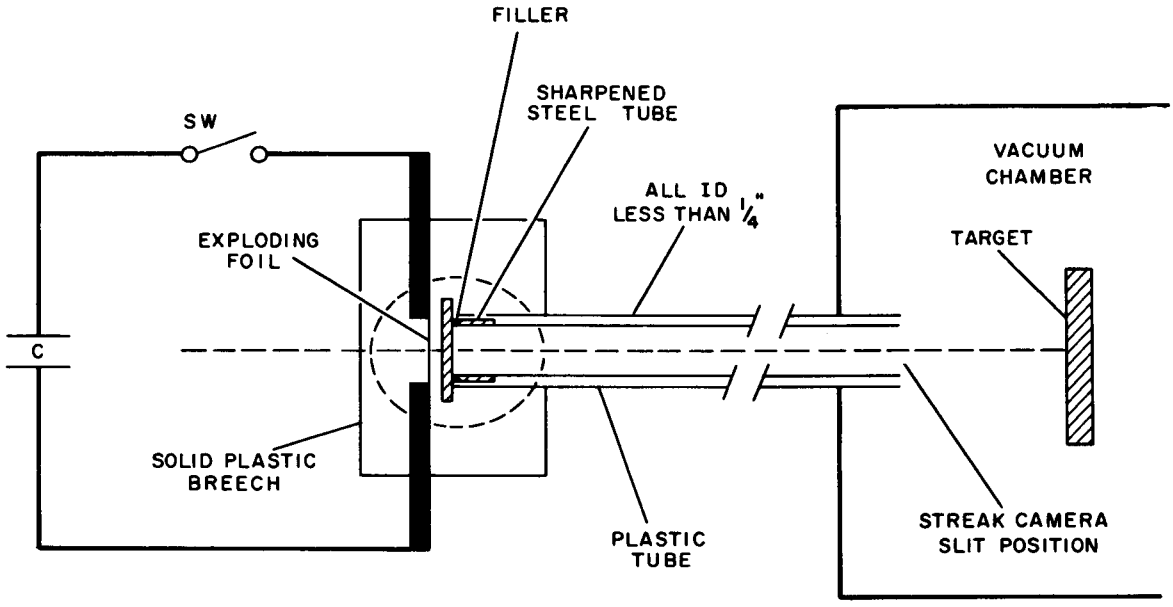

Figure 18. Special Gun for Small-Diameter, Disc-Shaped Particles

TARGET IMPACT

SPHERICAL PARTICLES

The research program on spherical particles was initiated with the gun shown in Figure 16. Numerous shots were fired using thick lead targets and spherical particles of copper and glass with the following diameters: 1/64 in., 1/32 in., 1/16 in. Wires and foils were exploded. Particle velocities were measured with the streak camera using methods described in Chapter 2. We investigated this gun to the limit of particle disintegration for each breech arrangement. Maximum particle velocities of approximately 10,000 ft/sec were observed before particle disintegration.

Difficulties in obtaining higher particle velocities with this geometry can be attributed to:

1. Difficulties in efficiently coupling the small area foil (or wire) transducer to the electrical system
2. High peak-pressure transients generated when the small mass load transducer is vaporized (this caused particle breakup)
3. Barrel friction
4. Susceptibility of spherical particle geometry to breakup during short-duration pulse, stress loading.

Because of the difficulties encountered with this gun design in obtaining the desired velocities, we investigated the one illustrated in Figure 16. This gun is a modification of our "standard gun." The modified gun has a spherical particle glued to the front surface of the rupture disc, or sabot. After acceleration through a distance d, the sabot is stopped by a steel aperture plate. The accelerated particle passes through the aperture plate and impacts the target. The distance d, while as large as possible, allows the particle to pass through reliably.

We expected this to be a good way of accelerating particles, since we have had good success in accelerating the rupture disc, or sabot, in other experiments. For some time, it appeared that we were having very good success with this arrangement. Sabot velocities in excess of 50, 000 ft/sec were observed, and good single-particle impacts in thick lead targets were obtained. However, an analysis of many craters from these impacts indicated that the crater volumes were smaller than expected when compared with other cratering data that we have taken in the velocity range from 40, 000 to 60, 000 ft/sec. These results are not conclusive, however, since the craters made by the spherical particles were very small, and the crater volume was calculated from the measured crater diameter. We assumed that the craters were hemispherical in shape.

Within the scope of this study, we could not put further effort into this work. There are several difficulties involved in such investigations. First, there is a good chance that the particle is shock-launched away from the sabot before the sabot

is accelerated. If this occurs, the particle will be accelerated to a velocity that is probably much lower than that of the sabot. Or the particle may be properly accelerated with the sabot, but may be slowed down when the sabot is stopped. Our method of measuring the particle velocity assumes that the particle has the same velocity as the sabot. If it does not, we do not presently have a method for measuring the particle velocity.

This method could be effectively improved in the following ways:

1. Establish methods of measuring particle velocity independently of plasma or sabot.
2. Carry out additional saboting studies, possibly using a conventional sabot in which the particle is clamped between restraining parts.

DISC-SHAPED PARTICLES

All the experimental particle-impact data presented in this report were obtained by impacting disc-shaped particles on 2024-T3 aluminum targets. For disc-shaped particles with diameters of 1/4 in., we used our standard gun geometry. For disc-shaped particles having diameters less than 1/4 in., the geometry shown in Figure 17 was used. For all cases, the particle mass just prior to impact was experimentally measured as described in Chapter 3.

The data for all shots are presented in Tables 1 to 3. For those conditions where sufficient data were obtained to plot curves, we have done so.

Mylar Particles Bombarding 2024-T3 Aluminum Targets

The data for Mylar particles bombarding aluminum targets are given in Table 2. We have tabulated the shot number, the particle shape and mass, the particle velocity, the crater volume, the ratio of crater volume to particle mass, and the crater depth.

The particle mass was measured by the methods described in Chapter 3. A large number of shots were fired (up to 25) and the values of the measured mass were averaged. The root mean square deviations were then calculated and these are given in Table 1. By firing at least 25 shots, the statistical deviations are reduced to

TABLE 2

SUMMARY OF MYLAR PARTICLE IMPACT DATA
ON 2024-T3 ALUMINUM TARGETS

Shot No.	Velocity (ft/sec x 10^4)	Crater Volume (cm^3)	$\frac{Vc}{m}$ (cm^3/gm)	Crater Depth (cm)
Mylar Disc: 0.0250 in. diameter, 0.010 in. thick, 6.06 ± 0.126 mg mass				
2758	3.82	0.033	5.45	0.284
2761	3.61	0.041	6.75	0.353
2762	2.76	0.031	5.1	0.236
2764	4.10	0.050	8.25	0.376
2769	3.65	0.048	7.9	0.410
2772	2.86	0.026	4.3	0.310
2852	3.30	0.024	3.96	0.270
2853	4.25	0.027	4.45	0.394
3239	4.40	0.054	8.9	0.266
3270	6.20	0.068	11.2	0.330
3271	5.20	0.045	7.4	0.231
3272	5.95	0.070	11.5	0.394
3273	5.30	0.042	6.9	0.415
3274	4.20	0.052	8.6	0.295
3275	5.55	0.057	9.4	0.354
Mylar Disc: 0.125 in. diameter, 0.010 in. thick, 1.43 ± 0.022 mg mass				
3278	5.55	0.012		0.190
3282	5.20	0.012		0.235
3283	4.90	0.009		0.308

a few per cent in all cases. This method does not take into account possible systematic errors that might be present. Two such possible systematic errors are:

1. Loss of target mass in the vacuum chamber prior to particle bombardment
2. Loss of blow-off momentum through the hole in the special target. This would cause our measurement of particle mass to be high.

In Figure 19, we plot the crater volume as a function of particle velocity for two sizes of Mylar particles. The top curve is for 6.06 mg particles and the bottom curve is for 1.43 mg particles. There is quite a bit of deviation of individual points

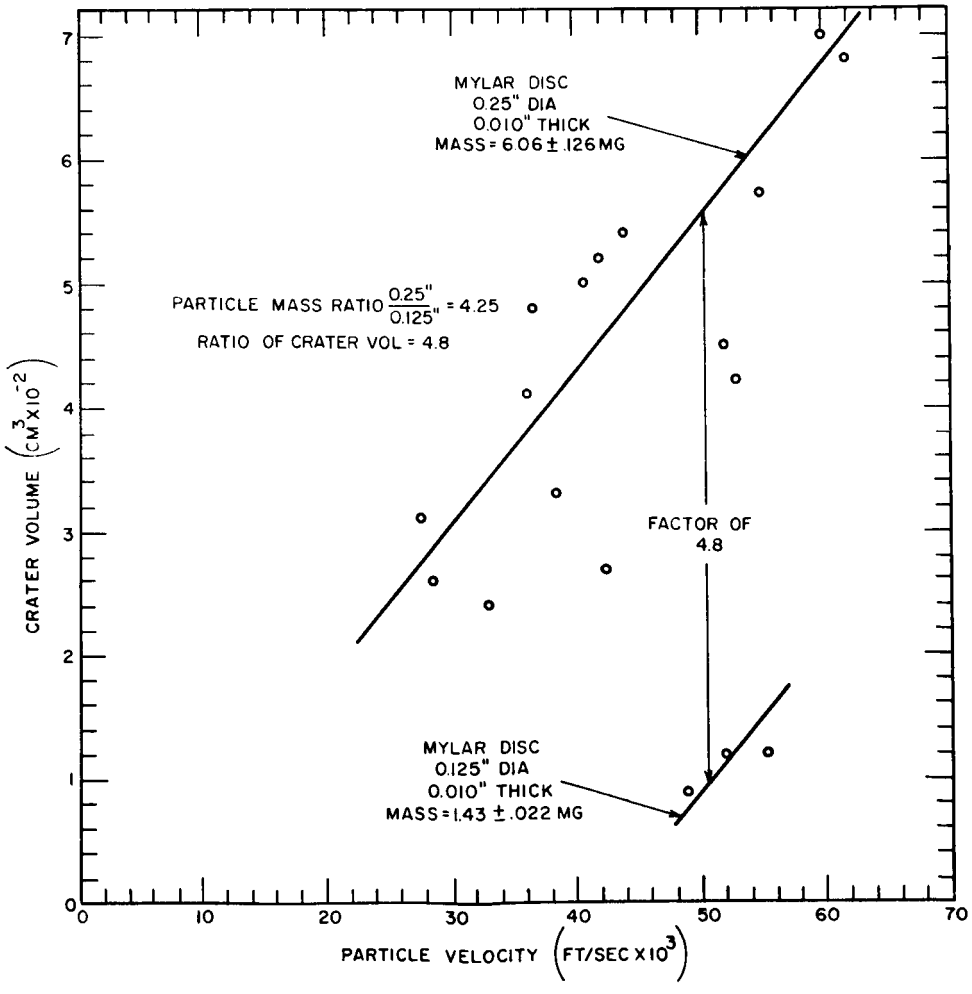

Figure 19. Crater Volume as a Function of Particle Velocity for Mylar Particles Impacting 2024-T3 Aluminum Targets

about the curves that have been drawn. These deviations can be attributed primarily to the following factors:

1. Front-surface spalling from the target. The amount of spalling might vary from shot to shot under similar impact conditions.
2. Measurement of crater volume. An error of about 5% can be attributed to this operation.
3. Measurement of impacting mass at the present time. A statistical deviation of several per cent is likely.
4. Measurement of particle velocity. The actual error in taking data from the film is only about 2.5%. Uncertainties in interpreting the film might raise the figure to about 20%.

It is interesting to note that the two curves shown in Figure 18 are separated in crater volume by a factor of 4.8. The measured ratio of impacting particle mass is 4.25.

Given the present state of the art in the field of hypervelocity impact phenomena, it is difficult to compare our data with that of other researchers in the field. Differences in conditions such as:

1. Projectile mass, shape, and composition
2. Target composition
3. Projection methods

make exact comparisons difficult. For small particles, even the surface treatment of the target could affect the cratering results.

However, we have made an attempt to compare our data with that taken at the Naval Research Laboratory and published recently.[1] The data used for comparison were copied from Ref. 1 and are presented in Figure 20. These data are the nearest to ours, in terms of particle velocity and target composition that we have readily available. Figure 20 shows a plot of crater volume vs particle kinetic energy for

[1] S. M. Halperson and W. W. Atkins, "Observations of Hypervelocity Impact," Proceedings of the Fifth Symposium on Hypervelocity Impact (April, 1962) vol. 1, pt. 2.

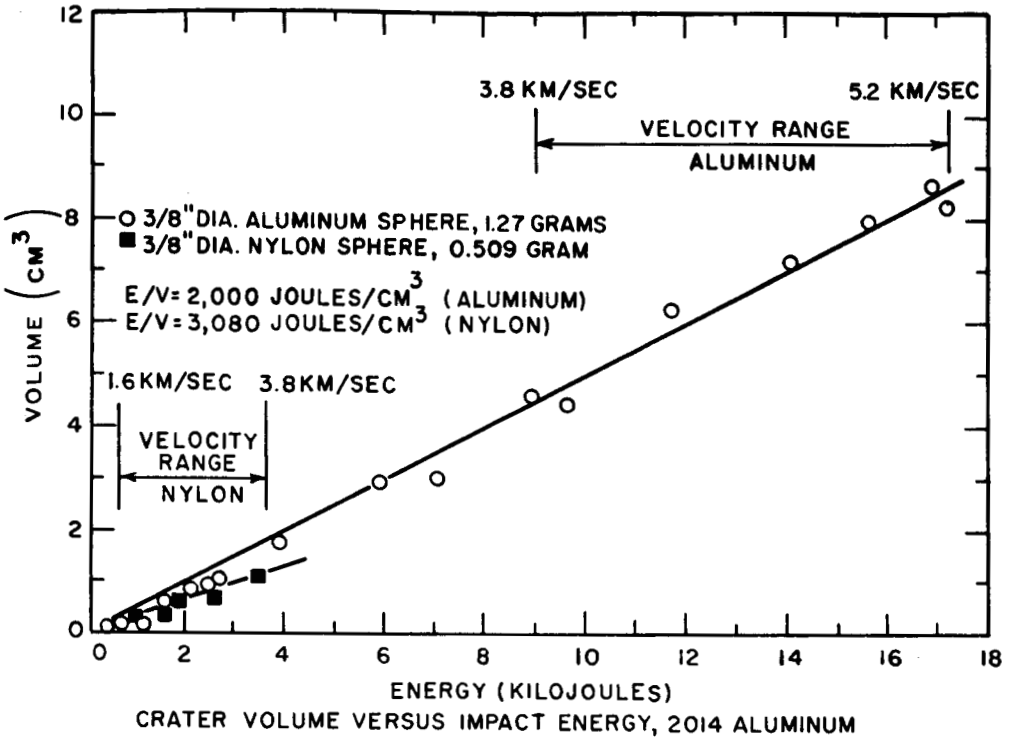

Figure 20. NRL Observations of Hypervelocity Impact
(Reprinted by Permission)

aluminum and Mylar spheres impacting 2014 aluminum targets. The data extend to a particle velocity of approximately 5.2 km/sec (18,000 ft/sec). We have transferred the data from Figure 19 to Figure 21 by taking points from the solid lines, and converting the information for plotting $\frac{\text{Crater volume}}{\text{Particle mass}}$ vs particle velocity. We transferred our data in a similar manner from Figure 19.

In comparing the data in Figure 21, we notice that NRL used 2014 aluminum targets, while we used 2024-T3 aluminum targets. The upper NRL curve is for aluminum particles and the bottom curve is for Nylon particles. Nylon particles should produce results similar to those for Mylar.

The depth of penetration measurement tabulated in Table 1 shows more variation than the crater volume measurement. This is due to the possibility that penetration is more sensitive than crater volume to particle orientation at the time of impact. In Figure 22, we have plotted the raw penetration data. Then we have averaged the circled points to obtain the square point shown in each circle.

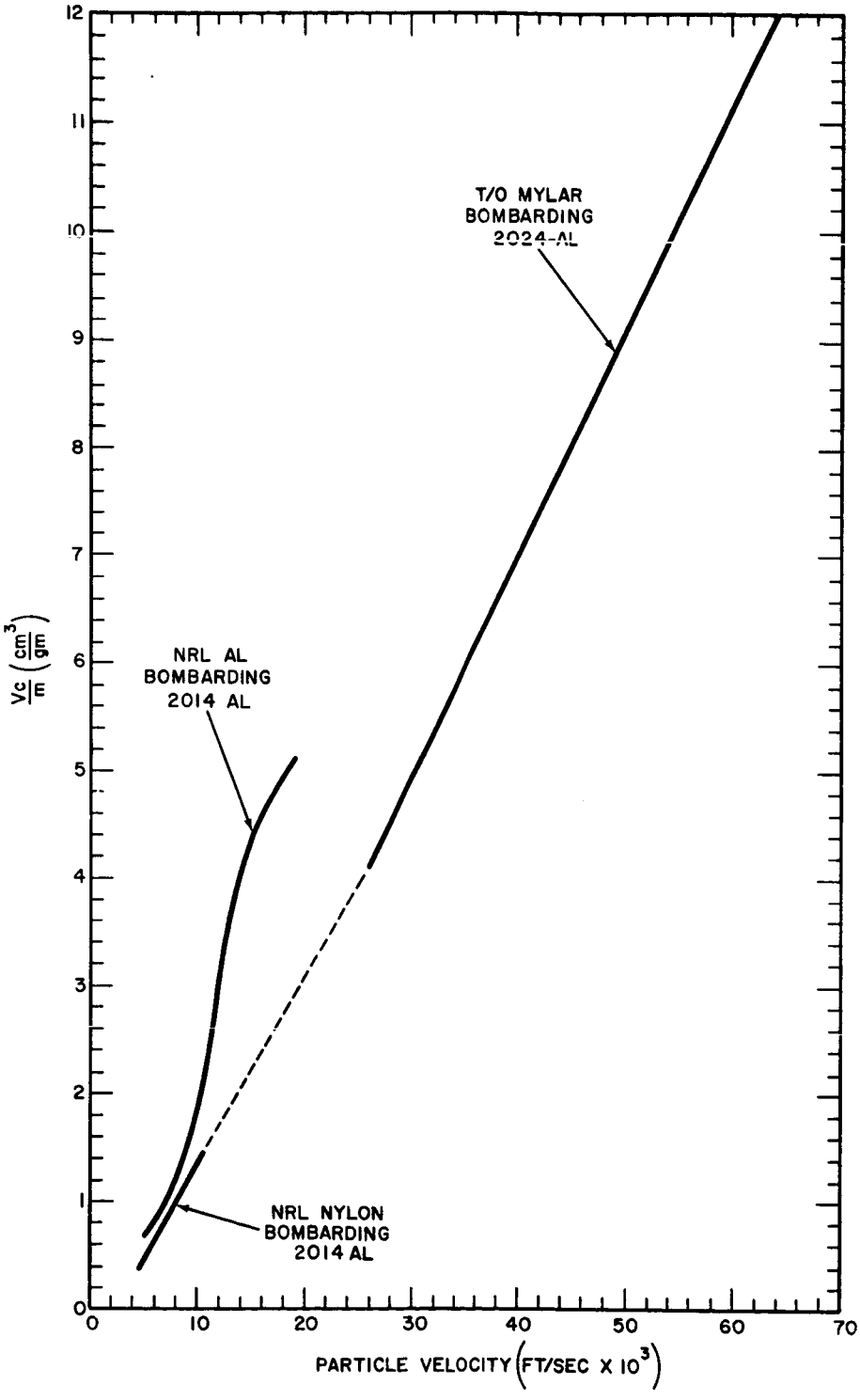

Figure 21. Comparison of Tech/Ops Data with NRL Data

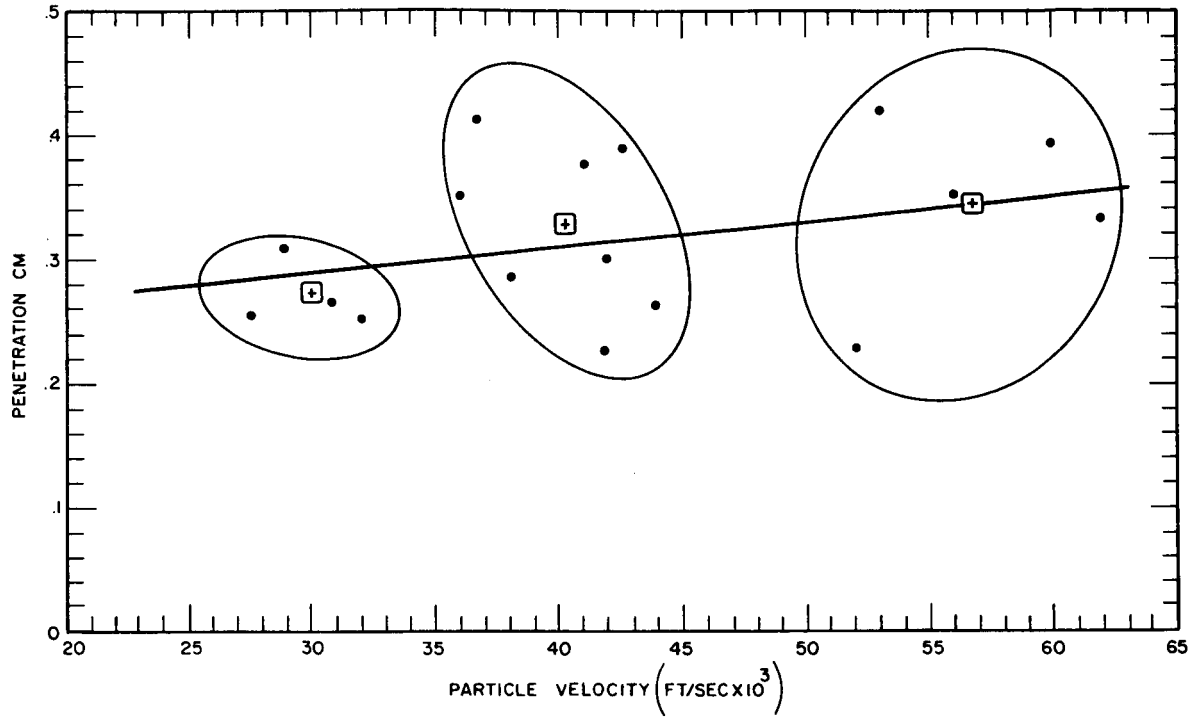

Figure 22. Depth of Penetration of Mylar Particles Bombarding 2024-T3 Aluminum Targets

Aluminum and Copper Particles

In Table 3, we have tabulated the results for aluminum particles impacting 2024-T3 aluminum targets. Sufficient data were not obtained for plotting. As before, we have tabulated the shot number, the particle velocity, crater volume, and crater depth.

In Table 4, we have tabulated the results for copper particles impacting aluminum targets. Sufficient data were not available for plotting.

TABLE 3

SUMMARY OF ALUMINUM PARTICLE IMPACT DATA
ON 2024-T3 ALUMINUM TARGETS

Shot No.	Velocity (ft/sec x 10^4)	Crater Volume (cm^3)	Crater Depth (cm)
Aluminum Disc: 0.250 in. diameter, 0.05 in. thick, 6.04 ± 0.545 mg mass			
2750	4.25	0.021	0.318
2821	4.43	0.013	0.374
2822	4.45	0.028	0.272
2823	5.10	0.030	0.353
2825	4.28	0.034	0.330
2830	4.96	0.028	0.330
2836	3.72	0.020	0.300

TABLE 4

SUMMARY OF COPPER PARTICLE IMPACT DATA
ON 2024-T3 ALUMINUM TARGETS

Shot No.	Velocity (ft/sec x 10^4)	Crater Volume (cm^3)	Crater Depth (cm)
Copper Disc: 0.250 in. diameter, 0.005 in. thick, 6.98 ± 0.890 mg mass			
2801	3.61	0.023	0.318
2802	—	0.023	0.310
2804	4.40	0.018	0.282
2809	4.63	0.018	0.190
2811	3.81	0.024	0.267
2814	3.52	0.019	0.188
Copper Disc: 0.120 in. diameter, 0.005 in. thick, 1.64 ± 0.16 mg mass			
2873	2.78	0.006	0.160
2882	3.32	0.008	0.152
2894	3.26	0.007	0.127
2898	1.73	0.005	0.137

CHAPTER 5

CONCLUSIONS AND RECOMMENDATIONS

While the experiments that were made to accelerate spherical particles were not sufficiently useful to carry out the required target impacts, we have had good results with disc-shaped particles. However, at least one of the methods of projecting spherical particles appears to be promising for further investigation. Better diagnostics than we presently have available will be required for this work. Disc-shaped particles having diameters as small as 0.080 in. have been successfully impacted. We recommend the use of small diameter discs for small mass particle work in the near future. Meanwhile, the difficulties encountered in accelerating spherical particles can be overcome.

For all work of the type reported here, a very intensive program of particle mass and velocity diagnostics are advisable.

We would like to initiate a program with objectives similar to those of this study but of sufficient magnitude to accomplish the following:

1. Fire sufficient numbers of shots to apply statistical analysis methods.
2. Carry out more extensive diagnostic measurements of particle mass and velocity so that the reliability of each data point is improved.
3. Extend the particle velocities to higher and lower values.